Research Square

Preprints are preliminary reports that have not undergone peer review.
They should not be considered conclusive, used to inform clinical practice,
or referenced by the media as validated information.

Ultrafast sintering of ultrafine-grained refractory metals at mild conditions

Lei Fu

leifu@whu.edu.cn

Wuhan University https://orcid.org/0000-0003-1356-4422

Erli Ni

Wuhan University

Jingrui Luo

Wuhan University

Yu Ding

Wuhan University

Zhujun Kuang

Wuhan University

Mengqi Zeng

Wuhan University https://orcid.org/0000-0002-1442-052X

Article

Keywords:

Posted Date: April 18th, 2025

DOI: https://doi.org/10.21203/rs.3.rs-6402284/v1

License: This work is licensed under a Creative Commons Attribution 4.0 International License.
Read Full License

Additional Declarations: There is **NO** Competing Interest.

Version of Record: A version of this preprint was published at Nature Materials on April 15th, 2026. See the published version at https://doi.org/10.1038/s41563-026-02587-6.

Abstract

Refractory metals are promising candidates in aerospace, energy conversion, and high-temperature structural materials due to their exceptionally high melting points, superior mechanical properties, and excellent chemical stability. However, their formidable melting temperature and machining difficulties derived from high delocalized electron densitypose a severe obstacle in the development of refractory metal structure materials by traditional manufacturing. Herein, we discovered that liquid metals with high efficiency in dissolving refractory metal atoms could significantly dilute the delocalized electron density, weaken metal bonding, and act as a fast diffusion medium, thus realizing the fabrication of refractory metal bulk materials at a significantly lower temperature (<1000 °C) in a very short time (~2 min). Based on the sintering mechanism, we achieved the general sintering of refractory metal bulks (including W, Re, Ta, Nb, Mo, V, Cr, and Ti). Most notable are the equiaxed ultrafine-grained microstructures with excellent mechanical properties. Additionally, this mild approach offers high flexibility for tunable compositions and mass manufacturing, enabling the production of refractory metal alloy, gradient structure material, and carbide-dispersion-strengthened alloy. This research represents a significant milestone in developing high-performance refractory structural materials.

Introduction

The harsh operating environments of aerospace, nuclear energy, and other fields require structural materials with excellent mechanical properties and high heat and corrosion resistance. Most materials fail or melt before they even reach operating temperature. Compared with the widely used nickel-based superalloys, refractory metals, such as tungsten (W), rhenium (Re), and molybdenum (Mo), have more advantages in high-temperature strength, microstructure stability, and resistance to irradiation damage[1–13]. Thus, developing fine microstructure refractory metal structural materials with high mechanical properties meets the needs of the ever-increasing service temperature and complex stress conditions. More importantly, refractory metals can expand the composition design space and superalloy systems to suit different applications under extreme environments.

These extraordinary properties of refractory metals arise from the strong metallic bonds in their crystalline structures, which are fundamentally driven by a high delocalized electron density. Delocalized electron density reflects the degree of free electron distribution within the crystal lattice, which, through the electron gas effect, significantly enhances interatomic bonding strength. While this high delocalized electron density confers outstanding thermal and mechanical stability, it also poses considerable challenges for the processing of these materials. Traditional processing and manufacturing methods have been used to produce various refractory metals available in product form[14–18]. However, these structural materials currently available for industrial and micro/nanoelectronics applications remain limited[19,20]. A major issue is that the formidable melting temperature of the refractory metal in excess of 2000 or even 3000 °C significantly challenges conventional metallurgy methods at high temperatures, such as melt casting, hot-pressed sintering (HP), two-step sintering (TSS), and spark plasma sintering

(SPS)[21]. The prolonged sintering process at high temperatures often ends up with coarse large grain sizes (abnormal grain growth), which significantly deteriorate the properties of materials. The root cause is that both densification and grain growth are driven by the capillary force and their thermally activated kinetics often have similar activation energies thus being difficult to separately control. Additionally, refractory metals exhibit poor plasticity at room temperature during severe plastic deformation (SPD) techniques such as high-pressure torsion (HPT), equal-channel angular pressing (ECAP), and surface mechanical attrition (SMA), limiting the development of fine-structured materials. Consequently, creating refractory metal materials with fine structures and desirable properties remains a significant challenge.

Here, we propose a novel approach involving the introduction of liquid metals to tailor the electronic structure of refractory metals. Liquid metals not only dilute the delocalized electron density of the refractory metals but also alter the distribution and uniformity of free electrons within the crystal lattice. We demonstrate the liquid metal-induced bond softening (LMIBS) strategy in which the weakened metallic bonding strength and promoted atom diffusion ensure the general synthesis of refractory metal structural materials at a significantly lower temperature (<1000 °C) in a very short time (~2 min). As demonstrated by Re and its alloy, the specimen possesses fine microstructures and excellent mechanical performance. Moreover, this mild approach is also versatile for tunable component and mass manufacturing, including refractory metal alloy, gradient structure material, and carbide-dispersion-strengthened Re alloys.

LMIBS sintering strategy

The first task to achieve the rapid activation sintering of refractory metal powder under significantly low temperatures ($0.3T_m$, T_m means melting temperature) is to solve the problem of the diffusion-migration of refractory metal atoms with high cohesive energy and stable crystal structure. In our strategy, we proposed the LMIBS route, which uses liquid metal as an accelerator for the diffusion of refractory metal atoms. Thereby, the overall fabrication process of the density refractory metal bulk could be primarily divided into three steps. Fig. 1a illustrates the typical manufacturing process of refractory metal bulk using the LMIBS sintering method. In the first step, refractory metal powders are compacted into cylindrical shapes by cold uniaxial pressing, breaking the arch bridge effect between particles. The powders fill pores and rearrange to increase contact points. In the second step, a small amount of liquid metal is evenly coated onto the refractory metal pellet, followed by brief heating below 800 °C to promote liquid metal penetration and compound formation at grain boundaries. In the final step, the liquid metal-permeated refractory metal pellet is sintered with ultrafast heating and cooling (Supplementary Fig. 1). The refractory metal matrix densifies, while liquid metal segregates to the surface and is removed using hydrochloric acid. The SEM images depict the process of refractory metals densifying (Supplementary Fig. 2 a-d). Initially, the pressed refractory metal pellet contains many voids and gaps. Liquid metal penetration gradually fills these voids and improves the spatial arrangement of the powders. After rapid sintering, grain boundaries coalesce, forming distinct sintering necks, which indicate the densification of the refractory metal bulk. Fig. 1b shows a schematic of the periodic table,

highlighting the refractory metal elements prepared using this method. The LMIBS sintering strategy can be ready to almost all accessible refractory metal elements, including but not limited to W (T_m=3422 °C), Re (T_m=3186 °C), tantalum (Ta, T_m=3017 °C), Mo (T_m=2623 °C), niobium (Nb, T_m=2477 °C), titanium (Ti, T_m=1668 °C), vanadium (V, T_m=1917 °C), chromium (Cr, T_m=1907 °C). As shown in Fig. 1c, the sintering temperature using the LMIBS method is about 70% lower than the melting temperature of all refractory metals, indicating that this strategy has an extremely low temperature, and extremely low equipment requirements, and can minimize the abnormal grain growth during the long high-temperature sintering process. Fig. 1d-o and supplementary Fig. 3 show the images and the powder X-ray diffraction (XRD) of various pure refractory metal sheets with about 18 mm diameter. Once the limitation of the size of laboratory equipment is overcome, the preparation of larger-size refractory metal bulks could also be achieved. XRD reveals the single-phase, high crystallinity body-centered-cubic (BCC) or hexagonal-close-packed (HCP) structure. It is worth noting that the liquid metal only acts as an accelerator of grain boundary diffusion and almost does not become a component of the bulk material. As shown in Supplementary Fig. 4 and Supplementary Fig. 5, inductively coupled plasma mass spectrometry (ICP-MS) energy-dispersive X-ray spectroscopy (EDS) mapping indicates all refractory metal bulk samples with very infinitesimal residues of Ga element.

Ultra-strong refractory metals bulk

The challenging sintering issue of refractory metals has frequently been attributed to the high melting temperatures, resulting in the obtaining of high-purity refractory metals bulk that must undergo the prolonged sintering process at high temperatures. Fig. 2a summarizes the literature data on the sintering temperature and time of pure refractory metals and refractory metals alloys[6,19,22–25]. Compared to the conventional metallurgy methods, our work demonstrates significant advantages in the ultrafast sintering time (~ 2 min) and a significantly lower temperature (~1000 °C). Here, we take Re as an example to investigate the microstructure and properties of the sample obtained by this sintering method. From the perspective of grain size stability, as shown in Fig. 2 b-e, the average grain size in the bulk remains almost unchanged after rapid sintering (average size changing from 384 nm to 377 nm). Therefore, to mitigate microstructural bifurcation, the LMIBS sintering approach is conducted at low temperatures with slow/suppressed coarsening kinetics while allowing for active grain boundary diffusion for densification by liquid metals. This approach could be viewed as a promising route to form bulk ultrafine-grained materials. Even more complex microstructures, such as gradient nanograined, gradient nanolaminated, gradient nanotwinned, and bimodal grain structures, could also be achieved by our morphology stability between powder and bulk. The challenges associated with rampant grain growth and significant residual porosity have been well resolved. The typical polycrystalline structures were composed of uniform ultrafine equiaxed grains by Scanning electron microscopy (SEM) image of the as-sintered sample (Supplementary Fig. 6). We conducted electron backscattered diffraction (EBSD) in Fig. 2f, which shows homogeneous microstructures with a random distribution of various oriented grains. In situ powder X-ray diffraction (XRD) was conducted to characterize the high-temperature

stability of the specimens further, revealing the same single-phase, high crystallinity hexagonal-close-packed (HCP) structure of Re at both room temperature and 1000 °C (Supplementary Fig. 7).

Moreover, we performed tensile testing and compared the yield strength against pure Re and conventional pure metal structural materials prepared by other methods to verify the effectiveness of our LMIBS strategy. The as-sintered sample and the samples after cold-rolling and recrystallization annealing were cut by electrical discharge machined (EDM) as dog bone-shaped specimens (Supplementary Fig. 8). Fig. 2g shows the engineering stress-strain curves of all specimens. Notably, the sample annealed for 120 min exhibits a high 0.2%-offset tensile yield strength of $\sigma_{0.2}$ = 1018.9 MPa, substantially higher than the yield strength of all current Re bulk, highlighting the great potential of the liquid metal preparation strategy to enhance mechanical properties. In addition, controlling heat treatments allowed us further to tailor the mechanical properties (Fig. 2g). A direct comparison of the tensile yield strength is given in Fig. 2h, clearly demonstrating the excellent strength of our Re specimens that surpasses those of other state-of-the-art pure metals materials[6,13,26–42].

The role of liquid metal

Powder solidification is widely recognized as a promising approach for producing bulk nanocrystalline and ultrafine crystalline materials. However, its development is hindered by significant grain growth and residual porosity, which limit its practical applications. LMIBS rapid sintering stands out as a transformative approach, effectively promoting grain boundary diffusion while suppressing grain coarsening. Furthermore, we analyzed the role of liquid metal in the sintering process. Fig. 3a illustrates the atomic-scale progression of preparing ultra-strong refractory metal structural materials using the liquid metal reaction system. As demonstrated with Re, the process begins with forming Re-Ga intermetallic compounds at 800 ℃. As shown in Fig 3b-c and Supplementary Fig. 9, the liquid metal selectively permeates the grain boundaries of the pressed Re pellet, forming the Re-Ga compound layer at the grain boundaries. DFT calculations were performed to provide more insights into the mechanism of the liquid metal Ga-weakened metal bonding process. The bond strength of the refractory metals-Ga was quantitatively discussed using the classical free-electron model, where the metallic bond strength is positively related to the free electrons in alloy systems. The electron localization function analysis of the studied refractory metals-Ga systems reveals that the electrons are more localized around the Ga atoms, suggesting a decrease in free electrons (Fig. 4d and Supplementary Fig. 10 and 11). The band structure analysis also demonstrates the decreased free electron after introducing Ga (Supplementary Figs. 12 and 13), which would weaken the metallic bonds of refractory metals. The bond strength of alloy systems is further quantified using metallic bond strength (MBS) as the descriptor. Compared with pure Re, Ga doping can reduce the number of free electrons and thus weaken the bond strength of Re-Re. Specifically, the MBS is reduced by 50 % in the $Re_{35}Ga_1$ system compared with that in Re_{36} (Fig. 4e). To verify the significant effect of liquid metal on the diffusion of rhenium atoms, the representative tilt grain boundary was constructed based on the coincidence site lattice model, and the crystallographic structure of the atomic model was shown in Supplementary Figs. 14, wherein Ga atoms were located in the interstitial sites of the grain boundary. At a simulated temperature of 1000 °C, the Re

atoms at pure grain boundaries exhibit minimal mobility, as they are strongly bound within the lattice due to their high cohesive energy and stable crystal structure. In contrast, introducing liquid metal significantly distorts the lattice, creating a more favorable environment for atomic diffusion. This distortion reduces the energy barrier for Re atom migration, enabling more efficient diffusion along the grain boundaries. To quantify the diffusion behavior, we calculated the mean square displacement (MSD) of Re atoms over time for various simulation models. The MSD provides a quantitative measure of atomic mobility, highlighting the influence of liquid metal on enhancing atomic diffusion. The presence of liquid metal at the grain boundaries serves as an efficient diffusion medium for Re atoms. As shown in Fig. 3f, the diffusion rate of Re atoms within the liquid-metal environment is approximately 13,000 times higher than its self-diffusion coefficient in pure Re. This remarkable enhancement underscores the critical role of liquid metal in overcoming diffusion limitations inherent to refractory metals. The accelerated diffusion of Re atoms facilitates the migration and coalescence of grain boundaries, leading to the formation of equiaxed-grained Re bulk material. This process ensures a uniform microstructure, which is essential for enhancing mechanical properties such as strength and ductility. Rapid cooling plays a dual role: it promotes the agglomeration and precipitation of Re atoms while simultaneously enabling the efficient removal of residual liquid metal. This step is crucial for ensuring the purity and structural integrity of the final Re material. To validate the hypothesis that liquid metals can be easily separated, we conducted ab initio molecular dynamics (AIMD) simulations (Supplementary Fig. 15). These simulations provide atomistic insights into the behavior of Re and Ga atoms during the cooling process. The simulations revealed that Re atoms, owing to their high cohesive energy, rapidly aggregate and precipitate from the liquid-metal solvent once released from the intermetallic compound lattice. Simultaneously, Ga atoms return to their liquid state, facilitating their separation from the Re bulk. Because rhenium is chemically inert to hydrochloric acid, the separated Ga can be easily dissolved and removed through acid treatment, yielding highly pure Re structural materials. This simple yet effective purification step ensures the practical viability of the LMIBS sintering process.

Tunable component design

Alloying is another prevalent way to tune the physical and mechanical properties of materials. We further demonstrate the potential of our method in tunable composition of refractory metals and mass manufacturing. The tunable composition design shown in this paper includes alloying, chemical composition gradients, and hard second-phase doping (Fig. 4a–c). The addition of Re in Mo can significantly improve the strength of the alloy while maintaining good plasticity. In addition, Re-50Mo alloy exhibits good compatibility with both nuclear fuel and alkali metal coolant. As shown in Fig. 4a, the Re-Mo binary alloy with uniform grain distribution was prepared during a low-temperature rapid sintering process assisted by the liquid metal reaction system. Moreover, this method also could be extended to fabricate various alloys with a gradient in composition and phase. During sintering, the compositional gradient can be controlled by changing the volume fraction of the powder mixture. Here, the compositional gradient structure material sintered by our route exhibited the heterogeneous structure of HCP phase Re and BCC phase Mo (Fig. 4b). Finally, this method also can effectively provide a solution for uniformly dispersed second-phase sintering. The carbide-dispersion-strengthened (CDS) alloys, with

outstanding resistance to both extreme heat and irradiation, have emerged as the frontrunners for the core structural materials used in severe operational environments. However, the prolonged high-temperature treatment in the traditional metallurgical method accelerates the atomic-scale contact and agglomerations of carbide nanoparticles in the matrix, hindering high-level mechanical properties in CDS systems. As a demonstration, we achieved a uniform dispersion of dense tungsten carbide (WC) nanoparticles in the Re matrix (Fig. 4c).

Mass manufacturing

The LMIBS approach enables the simultaneous co-sintering of multiple materials, providing a highly efficient and scalable solution for mass manufacturing. By reducing energy consumption and processing time, this method addresses key challenges faced by conventional sintering techniques. Using this technique, 10 rhenium (Re) pellets can be rapidly co-sintered in a compact 2×5 matrix setup, occupying an area of approximately 6 cm × 2 cm for pellets sized 10 mm each (Fig. 4d). This efficient spatial arrangement allows for increased throughput while minimizing workspace requirements. Moreover, this technique is capable of sintering structures with intricate and complex geometries, as demonstrated in Figure 4d. This flexibility is particularly advantageous for producing customized components with precision. This capability is significant because traditional powder metallurgy methods are often incompatible with the complex, highly detailed geometries produced by additive manufacturing. By bridging this gap, our approach opens new avenues for integrating sintering techniques with advanced shaping technologies. These sintered materials, exhibiting exceptional mechanical strength, corrosion resistance, and oxidation stability, are ideal for micro-components operating in extreme environments such as aerospace, nuclear energy, and high-temperature industrial applications. By integrating advanced shaping processes like 3D printing and metal injection molding, this method has the potential to produce highly complex 3D structures. Such integration could revolutionize the fabrication of multi-functional components for next-generation technologies. To demonstrate the scalability of our approach, we successfully synthesized four Re pellets in a single co-sintering process from their corresponding green bodies (Fig. 4e and f). This result highlights the method's potential for high-throughput production while maintaining material integrity. In comparison, spark plasma sintering (SPS), though regarded as a high-throughput method for fabricating bulk metal specimens, typically produces only one specimen over a time of 1–2 hours. This limitation significantly reduces its efficiency for mass production. Furthermore, SPS faces challenges in scalability, as parallel processing requires multiple expensive SPS systems, making it cost-prohibitive for large-scale manufacturing. By contrast, our method offers a cost-effective and practical alternative for achieving high-volume production.

Conclusions

In conclusion, we have successfully developed an LMIBS sintering approach that overcomes the longstanding processing challenges of refractory metals. Based on the essence of metal electronic structure, our strategy could weaken the interatomic metal bond strength by regulating delocalized electron density, thus achieving low temperature-formed refractory metals. This method enables the

rapid and efficient preparation of 8 types of refractory metals at significantly lower temperatures (~1000 °C) and ultrashort sintering times (~2 minutes), as demonstrated by rhenium (Re) and its alloys. By preserving fine microstructures, such as equiaxed ultrafine grains, the resulting materials exhibit exceptional mechanical properties, including a tensile yield strength of 1.02 GPa—surpassing the performance of conventional refractory metals. Furthermore, this versatile approach accommodates tunable compositions, gradient structures, and carbide-dispersion-strengthened systems, expanding its applicability to a wide range of metallic materials and advanced structural designs. Unlike traditional powder metallurgy techniques, which often sacrifice microstructural control and post-consolidation properties, our method ensures both densification and property optimization without compromise. This universal and scalable strategy not only broadens the application potential of refractory metals in extreme environments and high-performance systems but also provides a blueprint for enhancing the processing and mechanical properties of other metallic materials. By bridging the gap between efficiency, cost-effectiveness, and material performance, this work opens new avenues for designing and manufacturing advanced structural components across aerospace, nuclear energy, and other demanding industrial sectors. Future research building upon this strategy will undoubtedly further expand its impact and accelerate the development of next-generation high-performance materials.

Declarations

Data availability

The data that support the findings of this study are available from the corresponding authors on reasonable request.

Acknowledgments:

We thank the Center for Electron Microscopy at Wuhan University for their substantial supports to TEM work. The numerical calculations in this paper have been done on the supercomputing system in the Supercomputing Center of Wuhan University

Funding:

The research was supported by the Natural Science Foundation of China (Grants 22025303, 21991154, and 12172260).

Author contributions:

L.F. conceived the research concept. L.F. and M.Q.Z. supervised the research. E.L.N. and J.R.L. carried out the main experiments. E.L.N. conducted the simulations. Z.J.K carried out the Partial SEM characterization. L.F., M.Q.Z., and E.L.N. wrote and edited the manuscript. All the authors contributed to data analysis and scientific discussion.

Competing interests:

Authors declare that they have no competing interests.

References

1. Lu, Y. et al. Nanoscale ductile fracture and associated atomistic mechanisms in a body-centered cubic refractory metal. *Nat. Commun.* **14**, 5540 (2023).
2. Zhong, L., Zhang, Y., Wang, X., Zhu, T. & Mao, S.X. Atomic-scale observation of nucleation- and growth-controlled deformation twinning in body-centered cubic nanocrystals. *Nat. Commun.* **15**, 560 (2024).
3. Zhang, Y.-H., Ma, E., Sun, J. & Han, W.-Z. Unveiling the intrinsic rhenium effect in Tungsten. *Acta Mater.* **264**, 119586 (2024).
4. Wang, J. et al. In situ atomic-scale observation of twinning-dominated deformation in nanoscale body-centred cubic tungsten. *Nat. Mater.* **14**, 594–600 (2015).
5. Yu, J. et al. Printing Three-dimensional refractory metal patterns in ambient air: toward high temperature sensors. *Adv. Sci.* **10**, 2302479 (2023).
6. Chen, W. et al. Revealing the room temperature superplasticity in bulk recrystallized molybdenum. *Nat. Commun.* **14**, 8336 (2023).
7. Braun, J. et al. Molybdenum and tungsten manufactured by selective laser melting: Analysis of defect structure and solidification mechanisms. *Int. J. Refract. Met. H.* **84**, 104999 (2019).
8. Carlen, J.-C. & Bryskin, B.D. Cold-forming mechanisms and work-hardening rate for Rhenium. *Int. J. Refract. Met. H.* **11**, 343–349 (1992).
9. Schneider, S.J. High temperature thruster technology for spacecraft propulsion. *Acta Astronaut.* **28**, 115–125 (1992).
10. Seyda, J. et al. Mechanical properties and microscopic analysis of sintered rhenium subjected to monotonic tension and uniaxial fatigue. *Mater. Sci. Eng. A* **817**, 141343 (2021).
11. He, Y., Fang, Z., Li, B., Wang, C. & Mao, S.X. In-situ HRTEM observations of intermediate phase transformation in lattice reorientation in HCP rhenium. *J. Mater. Sci. Technol.* **206**, 15–25 (2025).
12. Lunk, H.-J., Drobot, D.V. & Hartl, H. Discovery, properties and applications of rhenium and its compounds. *ChemTexts* **7**, 6 (2021).
13. Wei, Z., Zhang, L., Li, X., Long, Y. & Qu, X. Effect of grain size on deformation behavior of pure rhenium. *Mater. Sci. Eng. A* **829**, 142170 (2022).
14. Mostafaei, A. et al. Additive manufacturing of nickel-based superalloys: A state-of-the-art review on process-structure-defect-property relationship. *Prog. Mater. Sci.* **136**, 101108 (2023).
15. Chen, K. et al. Rafting-enabled recovery avoids recrystallization in 3d-printing-repaired single-crystal superalloys. *Adv. Mater.* **32**, 1907164 (2020).
16. Lemberg, J.A. & Ritchie, R.O. Mo-Si-B alloys for ultrahigh-temperature structural applications. *Adv. Mater.* **24**, 3445–3480 (2012).
17. Schütze, M. Single-crystal performance boost. *Nat. Mater.* **15**, 823–824 (2016).

18. Zhang, L. et al. Powder metallurgy route to ultrafine-grained refractory metals. *Adv. Mater.* **35**, 2205807 (2023).
19. Que, Z. et al. Resolving the sintering conundrum of high-rhenium tungsten alloys. *J. Mater. Sci. Technol.* **166**, 78–85 (2023).
20. Wang, C. et al. A general method to synthesize and sinter bulk ceramics in seconds. *Science* **368**, 521–526 (2020).
21. Funch, C. V. & Proust, G. Laser-based additive manufacturing of refractory metals and their alloys: A review. *Addit. Manuf.* **94**, 104464 (2024).
22. Ivanov, E.Y., Suryanarayana, C. & Bryskin, B.D. Synthesis of a nanocrystalline W–25 wt.% Re alloy by mechanical alloying. *Mater. Sci. Eng. A* **251**, 255–261 (1998).
23. Li, X. et al. Pressureless two-step sintering of ultrafine-grained tungsten. *Acta Mater.* **186**, 116–123 (2020).
24. Dong, Z. et al. Preparation of ultra-fine grain W-Y_2O_3 alloy by an improved wet chemical method and two-step spark plasma sintering. *J. Alloys Compd.* **695**, 2969–2973 (2017).
25. Lee, G., McKittrick, J., Ivanov, E. & Olevsky, E.A. Densification mechanism and mechanical properties of tungsten powder consolidated by spark plasma sintering. *Int. J. Refract. Met. H.* **61**, 22–29 (2016).
26. Ruan, Q., Yang, M., Liu, W. & Godfrey, A. Plastic yielding and tensile strength of near-micrometer grain size pure iron. *Mater. Sci. Eng. A* **744**, 764–772 (2019).
27. Mao, D. et al. Bimodal-grain structure enables superior strength-ductility synergy of pure Al. *J. Alloys Compd.* **1000**, 175114 (2024).
28. Wang, G. et al. Developing high-strength ultrafine-grained pure Al via large-pass ECAP and post cryo-rolling. *J. Mater. Res. Technol.* **15**, 2419–2428 (2021).
29. Zhao, Y.H. et al. Simultaneously increasing the ductility and strength of ultra-fine-grained pure copper. *Adv. Mater.* **18**, 2949–2953 (2006).
30. Jadhav, S.D., Goossens, L.R., Kinds, Y., Hooreweder, B.V. & Vanmeensel, K. Laser-based powder bed fusion additive manufacturing of pure copper. *Addit. Manuf.* **42**, 101990 (2021).
31. Liu, Y. et al. Manufacturing of high strength and high conductivity copper with laser powder bed fusion. *Nat. Commun.* **15**, 1283 (2024).
32. Lu, L., Shen, Y., Chen, X., Qian, L. & Lu, K. Ultrahigh strength and high electrical conductivity in copper. *Science* **304**, 422–426 (2004).
33. Liu, X. et al. Microstructure and texture characteristics of pure Ti with a superior combination of strength and ductility. *Mater. Sci. Eng. A* **808**, 140915 (2021).
34. Li, D. et al. Enhanced strength in pure Ti via design of alternating coarse- and fine-grain layers. *Acta Mater.* **206**, 116627 (2021).
35. Issariyapat, A., Kariya, S., Shitara, K., Umeda, J. & Kondoh, K. Solute-induced near-isotropic performance of laser powder bed fusion manufactured pure titanium. *Addit. Manuf.* **56**, 102907

(2022).
36. Zhao, Y. et al. High tensile ductility and strength in bulk nanostructured nickel. *Adv. Mater.* **20**, 3028–3033 (2008).
37. Xiao, Y. et al. Ultrahigh strength ultrapure nanostructured nickel metal prepared via ultrafine anode scanning electrodeposition. *Mater. Design* **213**, 110339 (2022).
38. Rebesan, P. et al. Pure molybdenum manufactured by laser powder bed fusion: thermal and mechanical characterization at room and high temperature. *Addit. Manuf.* **47**, 102277 (2021).
39. Braun, J., Kaserer, L., Stajkovic, J., Kestler, H. & Leichtfried, G. Grain refinement mechanisms of alloying molybdenum with carbon manufactured by laser powder bed fusion. *Mater. Design* **215**, 110507 (2022).
40. Guo, M., Liu, K., Sun, J. & Gu, D. Laser powder bed fusion of a novel nano-modified tungsten alloy with refined microstructure and enhanced strength. *Mater. Sci. Eng. A* **843**, 143096 (2022).
41. Kan, X., Li, J., Zhong, J. & Suo, T. Tailoring the adiabatic shear susceptibility of pure tungsten via texture evolution. *Int. J. Plast.* **174**, 103909 (2024).
42. Su, H. et al. Research on high-temperature mechanical properties and microstructure of powder metallurgical rhenium. *Int. J. Refract. Met. H.* **106**, 105861 (2022).

Figures

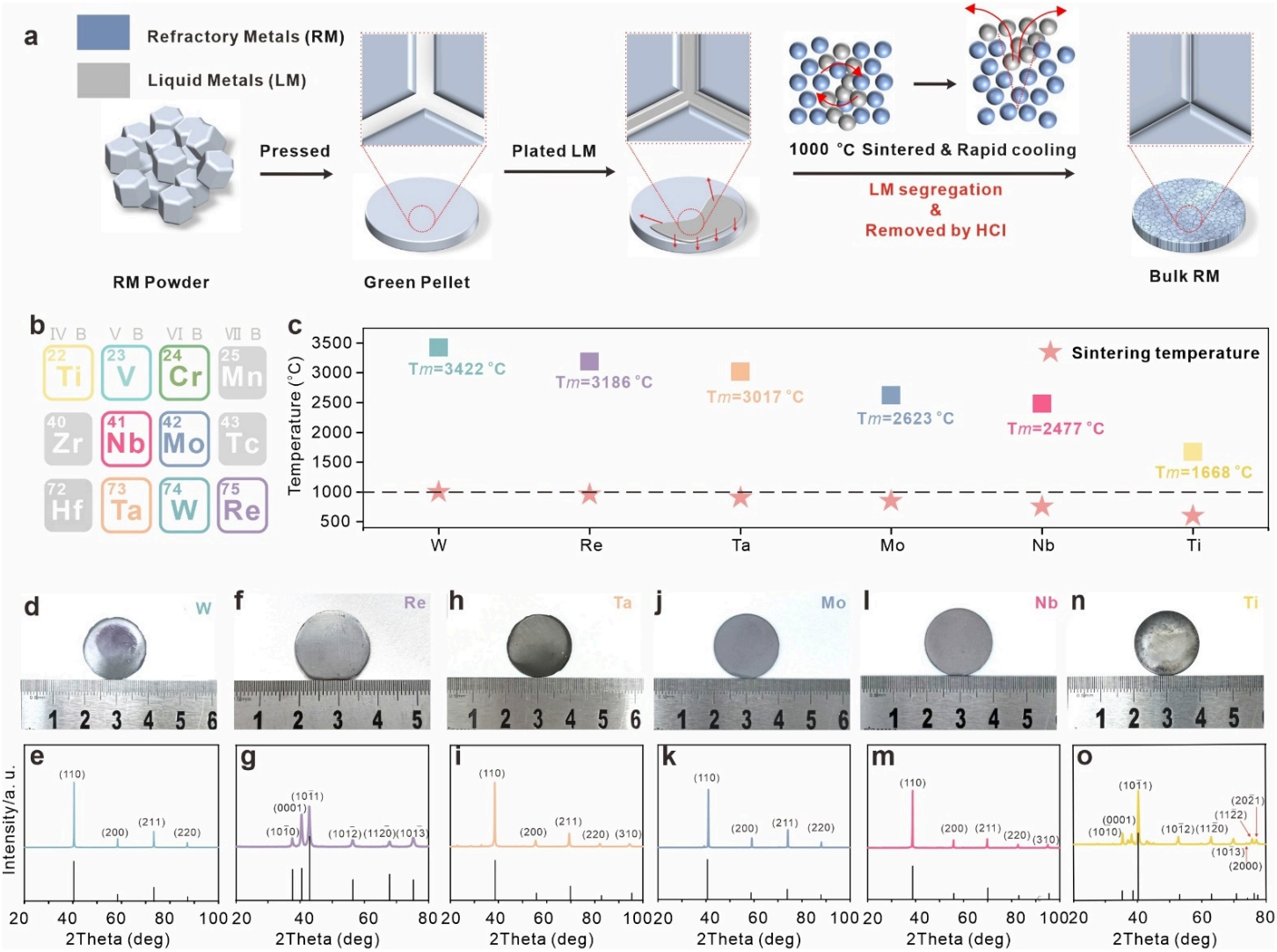

Figure 1

Typical manufacturing process and samples of the refractory metal bulk by the LMIBS sintering approach. a, Schematic illustration of the manufacturing process. **b**, Overview of metals that can prepared using the LMIBS route. **c**, Comparison of the temperature of the LMIBS sintering approach with melting temperature of the refractory metal. The limited temperature is 1000 °C for the LMIBS sintering approach. **d-o**, Optical images and XRD pattern of the 6 as-sinteredrefractory metal sheets. Contains: W, Re, Ta, Mo, Nb, Ti.

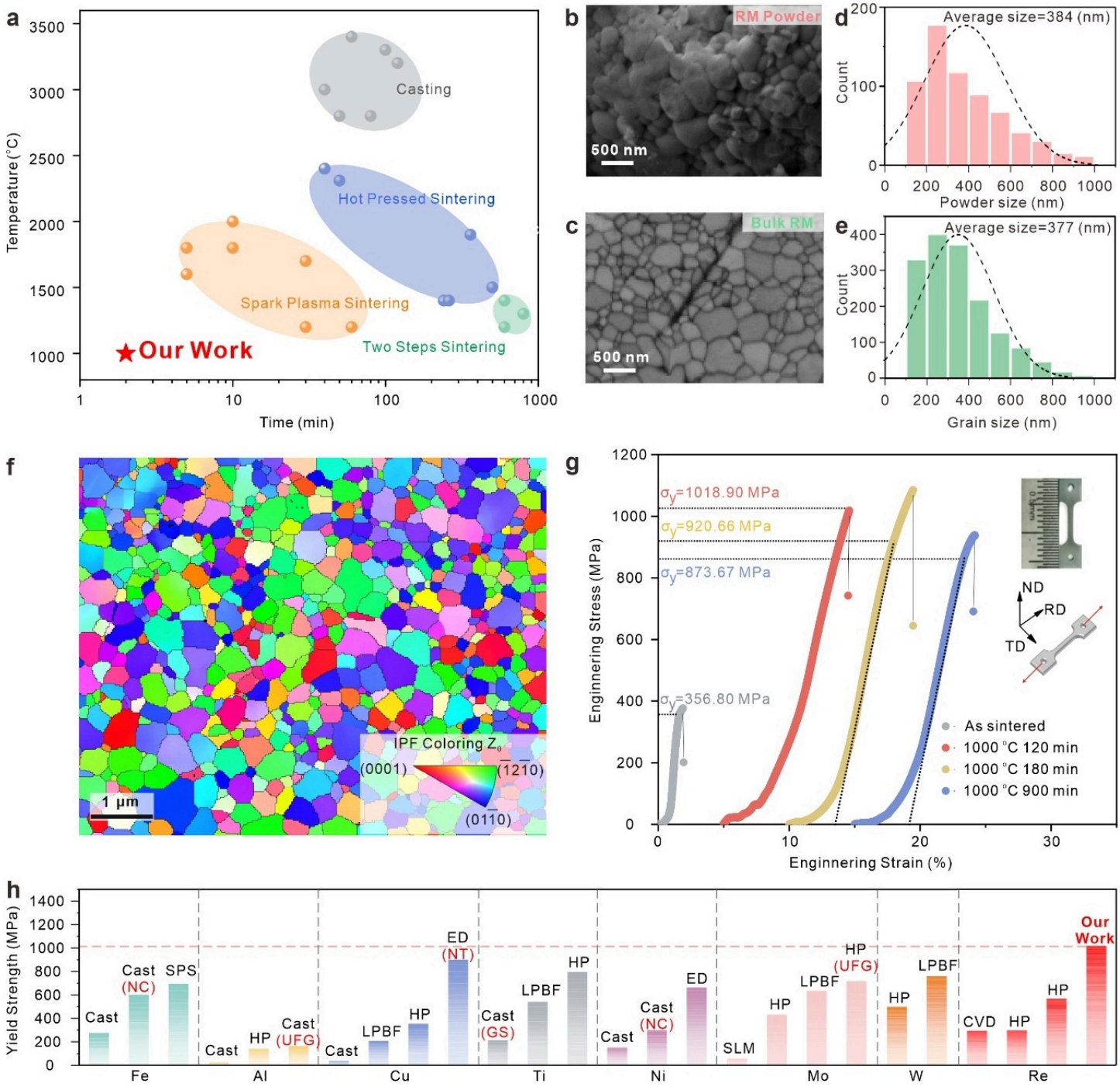

Figure 2

Structural characterization and mechanical properties of Re bulk. a, Ashby map in terms of the sintering time and the temperature of pure Re and Re alloys[6,19,22–25]. **b**, SEM image of the un-sintered refractory metal powders. **c**, SEM image of the refractory metal bulk after rapid sintering. **d-e**, Grain size distributions in **b** and **c**. **f**, Electron back-scattered diffraction (EBSD) results of the Re bulk showing the size and morphology of Re grains. IPF Z_0, inverse pole figure along z-axis direction. **g**, Tensile stress-strain curves of as-sintered and annealed Re bulks. The yield strengths (σ_y) are marked on the curves. The inset shows the photograph and schematic of a dogbone-shaped, the tensile direction is marked

with the red arrow. **h**, Comparison of yield strengths between our work and other state-of-the-art pure metal materials by conventional metallurgy method[6,13,26–42]. SPS, spark plasma sintering; HP, hot pressed sintering; LPBF, laser powder bed fusion; ED, electro-deposition; SLM, selective laser melting; CVD, chemical vapor deposition. NC, nano-crystals; UFG, ultra-fine grains; NT, nano-twinned.

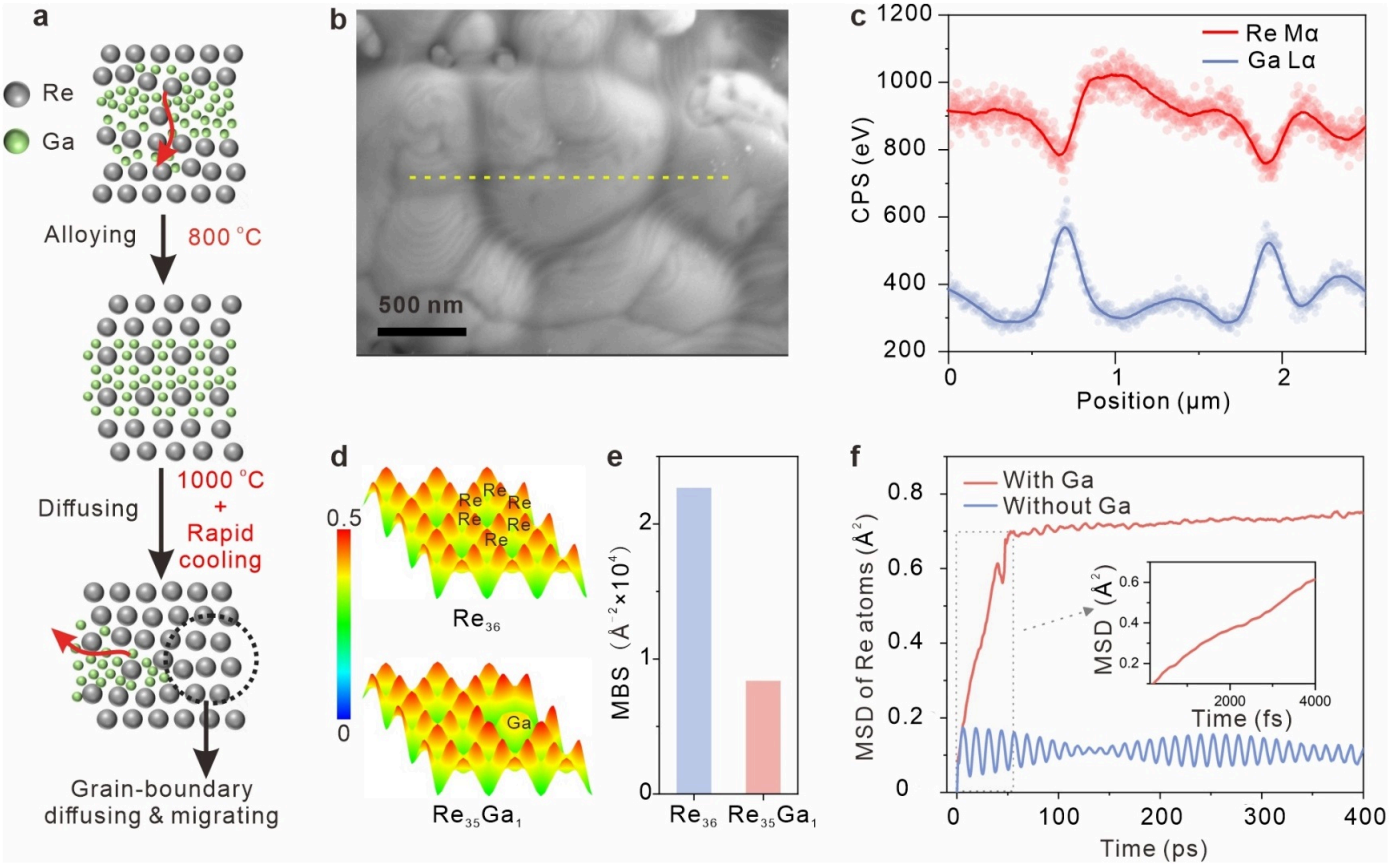

Figure 3

Mechanism analysis of the LMIBS approach of refractory metal. a, Schematic illustration of the general growth process for the production of ultra-strong Re structural materials by the liquid metal reaction system. **b**, Typical SEM image of microstructure after the liquid metal wet and permeates along the grain boundaries of the pressed green pellet. **c**, Line profiles of the count per second of individual elements taken from the respective EDS maps in b; each line profile represents the distribution of an element with different positions. **d**, There-dimensional display of the electron localization function analysis of the corresponding pure Re systems and Re-Ga systems. **e**, Statistic of the MBS values of the corresponding pure Re systems and Re-Ga systems. **f**, The MSD of Re atoms of Ga atoms or without Ga atoms between the grain boundaries model.

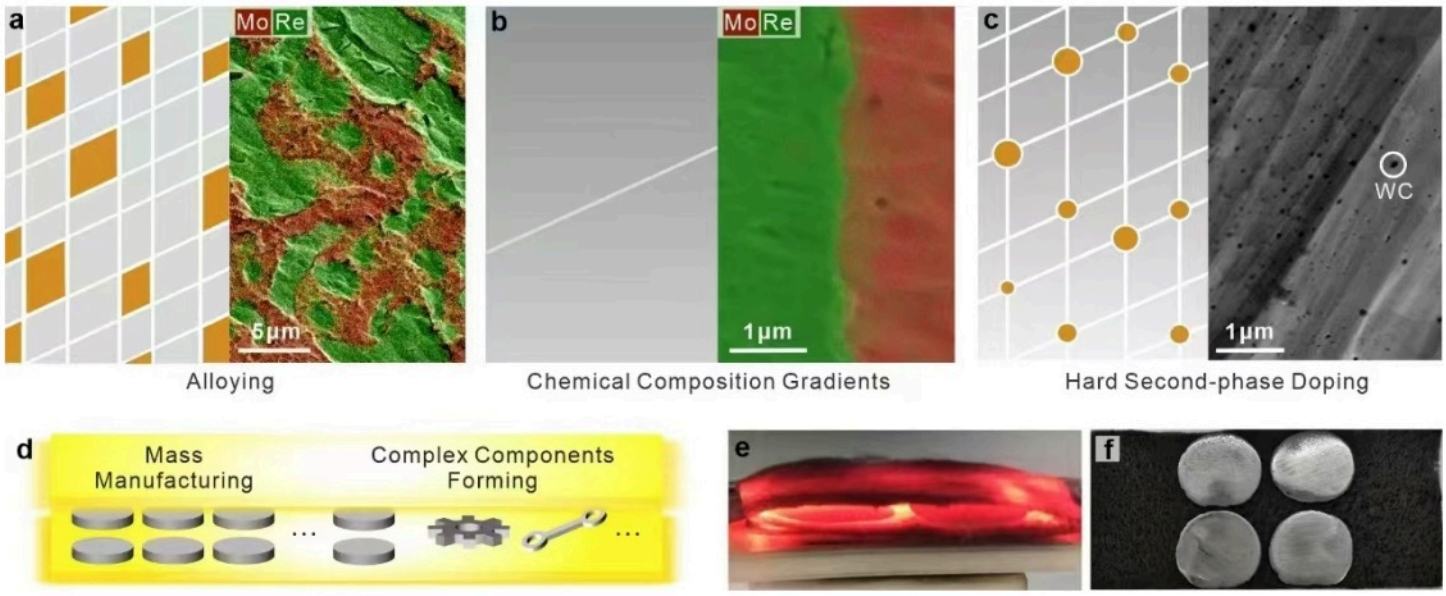

Figure 4

Tunable composition and mass manufacturing of refractory metals. a, Schematic and EDS mapping of the Re-50Mo alloy. **b**, Schematic and EDS mapping of the compositional gradient structure material.**c**, Schematic and SEM image of the carbide-dispersion-strengthened Re alloys. **d**, Schematic of a 2 by 5 matrix for cosintering 10 Re bulks and forming complex components. **e**, The side view of this methodcosintering process. **f**, Optical image of the co-sintering 4 Re pellets.

Supplementary Files

This is a list of supplementary files associated with this preprint. Click to download.

- supplementarymaterials.docx